J. Fluid Mech. (1997), *vol.* 338, *pp.* 277–297

Printed in the United Kingdom © 1997 Cambridge University Press

Miscible displacement between two parallel plates: BGK lattice gas simulations

By N. RAKOTOMALALA, D. SALIN AND P. WATZKY

Laboratoire Fluides, Automatique et Systèmes Thermiques, Université P.&M. Curie and Université Paris Sud, Bâtiment 502, Campus Universitaire, 91405 Orsay Cedex, France

(Received 29 February 1996 and in revised form 6 December 1996)

We study the displacement of miscible fluids between two parallel plates, for different values of the Péclet number *Pe* and of the viscosity ratio *M*. The full Navier–Stokes problem is addressed. As an alternative to the conventional finite difference methods, we use the BGK lattice gas method, which is well suited to miscible fluids and allows us to incorporate molecular diffusion at the microscopic scale of the lattice. This numerical experiment leads to a symmetric concentration profile about the middle of the gap between the plates; its shape is determined as a function of the Péclet number and the viscosity ratio. At *Pe* of the order of 1, mixing involves diffusion and advection in the flow direction. At large *Pe*, the fluids do not mix and an interface between them can be defined. Moreover, above $M \sim 10$, the interface becomes a well-defined finger, the reduced width of which tends to $\lambda_\infty = 0.56$ at large values of *M*. Assuming that miscible fluids at high *Pe* are similar to immiscible fluids at high capillary numbers, we find the analytical shape of that finger, using an extrapolation of the Reinelt–Saffman calculations for a Stokes immiscible flow. Surprisingly, the result is that our finger can be deduced from the famous Saffman–Taylor one, obtained in a potential flow, by a stretching in the flow direction by a factor of 2.12.

1. Introduction

When a fluid 1 displaces a more viscous fluid 2 ($M = \eta_2/\eta_1 > 1$), the interface between them is unstable (Saffman & Taylor 1958), leading to the so-called viscous fingering pattern, i.e. the penetration of a finger of the less-viscous fluid into the more-viscous one. This includes the well-known Saffman–Taylor finger in a Hele-Shaw cell, involving immiscible fluids, with no surface tension in Saffman & Taylor's pioneering work, as well as viscous fingering in porous media for miscible fluids without molecular diffusion (Bensimon *et al.* 1986; Hickernell & Yortsos 1986; Pelcé 1988; Yortsos & Hickernell 1989).

In the analysis of these two problems, an abrupt interface between the two fluids is assumed. Yet, dealing with miscible fluids is more subtle in a way: due to their mutual spreading, the finite interface width becomes a parameter of the instability, leading to new predictions, some of which have been verified in experiments (Manickam & Homsy 1995; Loggia *et al.* 1995). Curiously enough, the miscible problem has been mainly studied, both theoretically and experimentally (Wooding 1969; Homsy 1987; Bacri, Salin & Woumeni 1991; Bacri *et al.* 1992; Loggia *et al.* 1995), in the particular case of Darcy's flow in a porous medium, that is for a potential flow. Linear stability analysis and intensive computer simulations are based on a macroscopic convection–diffusion equation for the volume-averaged concentration,

https://doi.org/10.1017/S0022112097004928 Published online by Cambridge University Press

in which the hydrodynamic dispersion coefficient is assumed to be the one obtained from the dispersion of a passive tracer. Such an assumption is only exact in the case of Taylor (1953) and Aris (1956) passive dispersion: the mixing of the tracer is affected by the convective Haagen–Poiseuille velocity field, but remains a diffusive process. Note that the resolution of the tracer problem concerns also the case of two miscible fluids with the same viscosity and density. When the two fluids have different viscosities, their mixing leads to a viscosity distribution which modifies the velocity field. The flow field and concentration are then coupled, and the concept of the dispersion process should be questionable. Although the coupling has been analysed in heterogeneous porous media (Yortsos 1995), the understanding of the physical process of mixing in geometries as simple as a capillary tube or the space between two parallel plates (that is the gap of a Hele-Shaw cell), is still needed. Experiments in a capillary tube, involving miscible fluids of different viscosities, have been undertaken by Paterson (1985) and more recently by Petitjeans & Maxworthy (1996), as well as the corresponding simulations by Chen & Meiburg (1996). The viscous flow in the gap of a Hele-Shaw cell has been investigated by Yang & Yortsos (1997), in the asymptotic limit of an infinitely narrow gap and in the absence of diffusion. The immiscible displacement counterpart has been analysed by Reinelt & Saffman (1985), when capillary and viscous forces are comparable.

In the present paper, we tackle the issue of a miscible displacement in the gap of a Hele-Shaw cell, using a two-dimensional BGK lattice gas method. Such a method has been proved useful to simulate the complete Navier–Stokes equation (Qian, d'Humières & Lallemand 1992; Behrend, Harris & Warren 1994). The BGK approximation also provides a suitable way to incorporate molecular diffusion (Flekkøy 1993). Dealing with miscible fluids is then straightforward: the two fluids mix at the lattice scale. Moreover, viscosities, molecular diffusion, as well as mixing rules are directly introduced as independent tunable parameters. This allows us to cover a wide range of dynamic viscosity ratios and Péclet numbers (ratio of the characteristic diffusion time to the characteristic advection time).

After a brief review of the main lattice gases principles, with a particular focus on the miscible BGK model we shall use here, the results for the classical Taylor dispersion are presented, as a validity test of our scheme. Then we analyse a wide range of viscosity ratios M and Péclet numbers. At large Péclet numbers, molecular diffusion becomes negligible, and the mixing zone (i.e. the region between the pure fluids) remains narrow. In this limit, which should coincide with the limit of zero surface tension for immiscible fluids, our data exhibit a well-defined interface between the fluids. We study the shape of this interface versus M, and find that in the limit of large M, a steady-state-shaped finger is obtained. Finally we derive its analytical shape (Rakotomalala, Salin & Watzky 1996*a*).

2. Lattice gases

Basically, in the kinetic gas theory, simple collisions, preserving mass and momentum, are able to generate gas transport properties such as viscosity, mass and thermal diffusions. Statistical physics (Landau & Lifschitz 1958; Reif 1965), taking multiple collisions and interactions into account, leads to a more elaborated description of the fluid state. The essence of lattice gas modelling is to perform this statistical physics on a lattice with enough degrees of symmetry and freedom: a microscopic description of the (quasi-)particles movements and collisions will develop the macroscopic behaviour of the fluid. Thus, unlike classical discretization methods (finite elements,

https://doi.org/10.1017/S0022112097004928 Published online by Cambridge University Press

finite volumes, etc.), lattice gases are not *solvers* but *generators* of the Navier–Stokes equation. Since the pioneering work of Frisch, Hasslacher & Pomeau (1986) ten years ago, who demonstrated the ability of lattice gases to recover the complete Navier–Stokes equation, an extended literature has been written, applying this type of modelization to multiple systems with various complexity (Chen, Ohashi & Akiyama 1994; Ladd 1994*a*,*b*; Appert & d'Humières 1995). A thorough introduction and an exhaustive bibliography on lattice gases applications can be found in Benzi, Succi & Vergassola (1992) and Rothman & Zaleski (1994). Among the different lattice gas-related techniques that can be used to address a hydrodynamic problem, we have chosen the lattice BGK model, well suited to miscible fluids, since it allows us to easily incorporate molecular diffusion. We have superimposed a fluid mixing rule on the scheme, in order to account for the viscosity changes as mixing proceeds.

2.1. *The Lattice BGK model*

Following the statistical physics idea of Bhatnagar, Gross & Krook (1954), Qian (1990) and Qian *et al.* (1992) developed the lattice BGK model from the classical lattice-Boltzmann scheme of McNamara & Zanetti (1988) and Higuera & Jimenez (1989). The method uses square lattices in two dimensions. The space is represented by a regular grid (the node $\boldsymbol{r}$ and the direction vectors $\boldsymbol{e}_i$ connecting $\boldsymbol{r}$ to neighbours). According to Qian, the time evolution of the mass density $N_i(\boldsymbol{r}, t)$ in the direction i at time $t+1$ is

$$N_i(\boldsymbol{r}+\boldsymbol{e}_i, t+1) = N_i(\boldsymbol{r}, t) + \lambda_v N_i^{neq}(\boldsymbol{r}, t) \quad \text{where} \quad \lambda_v \in]-2, 0[. \tag{2.1}$$

λ_v is the viscosity relaxation parameter and N_i^{neq} the non-equilibrium part of the density probability distribution, given by

$$N_i^{neq} = N_i - N_i^{eq}. \tag{2.2}$$

To obtain the Navier–Stokes equation, the following equilibrium distribution is used for the local density $N_i^{eq}(\boldsymbol{r}, t)$:

$$N_i^{eq}(\boldsymbol{r}, t) = t_i \rho \left\{ 1 + \frac{e_{i\alpha} u_\alpha}{c_s^2} + \frac{u_\alpha u_\beta}{2c_s^2} \left(\frac{e_{i\alpha} e_{i\beta}}{c_s^2} - \delta_{\alpha\beta} \right) \right\}, \tag{2.3}$$

where c_s is the sound velocity, the greek subscripts indicate the Cartesian coordinates, with implicit summation on the repeated ones, and t_i are weighting parameters for each direction of the lattice, chosen so that the local mass and density be conserved without causing violation of the Galilean invariance. The physical variables are defined as

$$\rho = \sum_i N_i, \tag{2.4}$$

$$\rho \boldsymbol{u} = \sum_i \boldsymbol{e}_i N_i, \tag{2.5}$$

for respectively the mass and momentum densities per site.

Using a Chapman–Enskog multiscale technique, equation (2.1) gives the Newtonian incompressible Navier–Stokes equation:

$$\frac{\partial \boldsymbol{u}}{\partial t} + (\boldsymbol{u} \cdot \nabla)\boldsymbol{u} = -\frac{1}{\rho} \nabla P + \nu \, \Delta \boldsymbol{u}, \tag{2.6}$$

where the kinematic viscosity ν is linked to the relaxation parameter λ_v through the

https://doi.org/10.1017/S0022112097004928 Published online by Cambridge University Press

relation:

$$v = -\frac{1}{3}\left(\frac{1}{\lambda_v} + \frac{1}{2}\right). \tag{2.7}$$

2.2. *BGK lattice gas model for miscible fluids*

Dealing with miscible fluids (Flekkøy 1993) requires introducing molecular diffusion in a way which leads to a convection–diffusion equation for the concentration $C(\boldsymbol{r}, t)$ of one of the fluids. Let the fluids have the same viscosity (tracer case). The time evolution of the concentration in the direction i at time $t+1$ is given by

$$C_i(\boldsymbol{r} + \boldsymbol{e}_i, t+1) = C_i(\boldsymbol{r}, t) + \lambda_D C_i^{neq}(\boldsymbol{r}, t) \quad \text{where} \quad \lambda_D \in]-2, 0[, \tag{2.8}$$

with a simpler (scalar) equilibrium local concentration $C_i^{neq} = C_i - C_i^{eq}$:

$$C_i^{eq}(\boldsymbol{r}, t) = t_i C \left\{1 + \frac{e_{i\alpha} u_\alpha}{c_s^2}\right\}, \tag{2.9}$$

involving the local concentration $C = \sum_i C_i$. The molecular diffusion coefficient D_m is linked to λ_D through

$$D_m = -c_s^2 \left(\frac{1}{\lambda_D} + \frac{1}{2}\right). \tag{2.10}$$

Using the multiscale technique, the convection–diffusion equation is recovered:

$$\frac{\partial C}{\partial t} + \boldsymbol{u} \cdot \nabla C = D_m \Delta C. \tag{2.11}$$

The extension of the BGK method to a scalar quantity has been successfully tested (Flekkøy *et al.* 1995). It describes the dispersion of a passive tracer in a flow field (Taylor 1953).

When the tracer is active, i.e. in our case, when the two fluids do not have the same viscosity, the concentration-dependent properties of the mixture change as mixing occurs. We need therefore to implement a mixing rule for the viscosity (we do not address in this paper gravitational effects). This is carried out using a local viscosity which depends on concentration, $\eta[C(\boldsymbol{r}, t)]$. Then, according to the local concentration value $C(\boldsymbol{r}, t)$, the dynamic viscosity has a local value $\eta(\boldsymbol{r}, t)$, leading to a local kinematic viscosity $v(\boldsymbol{r}, t) = \eta(\boldsymbol{r}, t)/\rho$, and to a local relaxation parameter $\lambda_v(\boldsymbol{r}, t)$. With such a procedure, the Navier–Stokes equation and the convection–diffusion equation are coupled through the concentration-dependent viscosity: the velocity field and concentration depend on each other. Note that this scheme can be applied as well to non-Newtonian fluids, the effective kinematic viscosity to be put into the relaxation equation (2.1) becoming a function of the shear rate (Rakotomalala, Salin & Watzky 1996*b*).

2.3. *Simulations*

The simulations are performed on the so-called D2Q9 lattice (for two dimensions and nine lattice directions). The nine directions are the four medians and the four diagonals plus the centre of the square (figure 1), and the t_i have the following values:

$$t_0 = \tfrac{4}{9}; \quad t_1 = t_3 = t_5 = t_7 = \tfrac{1}{9}; \quad t_2 = t_4 = t_6 = t_8 = \tfrac{1}{36}. \tag{2.12}$$

https://doi.org/10.1017/S0022112097004928 Published online by Cambridge University Press

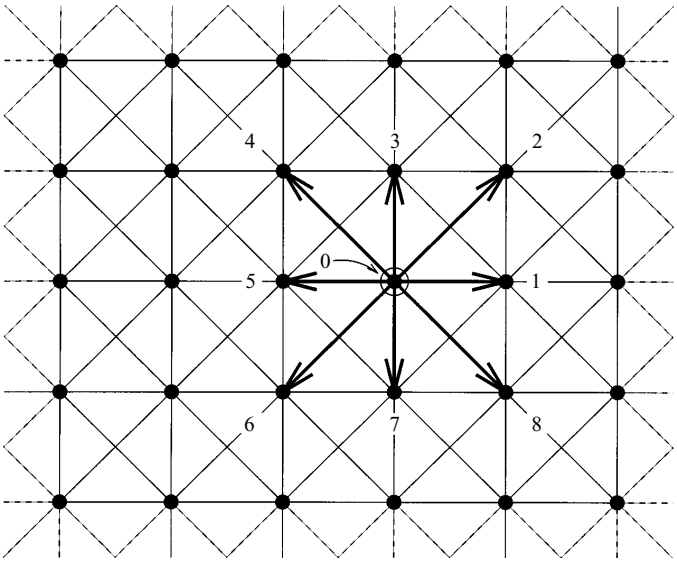


FIGURE 1. The D2Q9 lattice and the lattices links $\boldsymbol{e}_i$.

The sound velocity is $c_s = 1/\sqrt{3}$. We use an exponential mixing rule close to experiments, and also used in other simulations (Homsy 1987):

$$\eta(C) = \eta(0)\exp(-C\log M) \quad \text{where} \quad M = \frac{\eta_2}{\eta_1},\ \eta(0) = \eta_2,\ \eta(1) = \eta_1. \tag{2.13}$$

Accessible kinematic viscosities and diffusion coefficients range between 10^{-4} and 1. Larger values for the viscosity (i.e. $\lambda_v > -0.29$) lead to a strong shear near the wall boundaries and the no-slip condition (through a simple bounceback routine) cannot be ensured, unless a larger lattice is used. When this is the case, more sophisticated boundary conditions have to be introduced (Inamuro, Yoshino & Ogino 1995). On the other hand, a value smaller than 10^{-4} can lead to a prohibitive equilibrium time and to numerical instability. For those reasons, the kinematic viscosity has been varied between 5×10^{-4} and 0.5, and the molecular diffusion coefficient between 10^{-4} and 0.1. The lattice size is $y \times x = H \times L = N_y \times N_x = 32 \times 256$. One of the simulations presented in this work has been performed on a narrower and much longer lattice ($H = 16$, $L = 2048$), in order to ensure a good description of the macroscopic flow. The robustness of our results has been tested successfully with longer and wider lattices (from 16×2048 to 64×512), while keeping the same characteristic dimensionless numbers (Reynolds and Péclet numbers defined below). Our choice of the value $H = 32$ throughout this work is a compromise between the computational time efficiency and having a sufficient amount of points in order to smooth the profiles diagrams. Our algorithms are implemented on parallel machines (CM5 and Cray-T3D). Parallelism is definitely suitable for lattice modelling, owing to the independence of each node: collision and propagation steps can be achieved simultaneously at all nodes. For a 32×256 lattice, and 20 000 time steps, the typical computing time is respectively 15 and 3 CPU minutes for a 32 nodes-partition of a CM5 computer and of a Cray-T3D.

In the simulations, the fluids are initially at rest with a flat interface at the reduced position $x/L = 0.1$. The flow is then switched on, like in laboratory experiments;

https://doi.org/10.1017/S0022112097004928 Published online by Cambridge University Press

the average fluid velocity along the direction x is kept constant and equal to U_0. The characteristic dimensionless numbers of our problem are the viscosity ratio $M = \eta_2/\eta_1$, η_2 and η_1 being the viscosities of the displaced fluid and of the injected one, respectively, the Reynolds number $Re = U_0 H/v$ and the Péclet number, defined by $Pe = U_0 H^2/l\ D_m$, where l is the extent of the injected fluid in the flow direction, at a given time τ_C ($l = U_0\ \tau_C$). The Péclet number defined in this way is the ratio of the typical transverse diffusion time $\tau_{D_m} \sim H^2/D_m$ to the typical advection one $\tau_C \sim l/U_0$ over the distance l. When Pe is much greater than 1, molecular diffusion is negligible: the injected fluid has not enough time to diffuse transversely, whereas it has been advected in the meantime by a distance l in the flow direction. One of our aims in the following sections will be to study the flow pattern obtained at large Péclet numbers: in order to do this, one may choose a large average velocity (yet it has to be much smaller than the sound velocity) and a small diffusion coefficient (not smaller than roughly 10^{-4}). The Péclet number obtained in this way may be large at the beginning of the simulation, but it will decrease as time evolves (since $Pe \propto 1/\tau_C$), giving an increasing emphasis on diffusion. Another important number is the characteristic viscous diffusion time over the cross-section, $\tau_v \sim H^2/4v$, related to entrance effects. In order to avoid these effects, the following inequality has to be verified: $\tau_v < \tau_C$, which implies that Pe be smaller than $Pe^* = 4v/D_m$. The viscosity ratio M has been varied between 0.01 and 1000. The Reynolds number is of the order of 1 for M ranging between 0.1 and 10; for the extreme cases ($M = 0.01$ and $M = 1000$), it is of the order of 1 or 100, according to whether the viscosity used in its evaluation is that of the displaced fluid or the injected one. The Péclet number ranges between 0.5 and 512. The Reynolds and Péclet numbers are varied independently with the transport coefficients, v and D_m respectively, the average velocity U_0 and the lattice width H remaining constant, and equal to 0.005 and 32 respectively, unless specified. Note that real variables (denoted by R) are related to lattice variables as follows: let l_0 be the lattice spacing (i.e. $l_0 = L/N_x$), and t_0 the time step, $u_R = u\ l_0/t_0$, $v_R = v\ l_0^2\ /\ t_0$,... For each simulation, we shall present a data set of the normalized longitudinal velocity field $u_x(\boldsymbol{r}, t)/U_0$, the iso-concentrations $C = 0.25, 0.5, 0.75$ and the transverse-averaged concentration profile at different time steps:

$$\bar{C}(x,t) = \frac{1}{H}\int_0^H C(x,y,t)\,\mathrm{d}y. \tag{2.14}$$

3. Results and discussion

3.1. *Case $M = 1$: the effect of molecular diffusion*

The so-called Taylor–Aris hydrodynamic dispersion model (Taylor 1953; Aris 1956) describing the mixing in a tube or between two parallel plates represents a convenient way to validate a flow simulation (Baudet *et al.* 1989). Basically, the mixing of two miscible fluids is the result of the interplay between molecular diffusion and the advection by the flow. For fluids of equal viscosities, the velocity field $\boldsymbol{u}(\boldsymbol{r})$ is a Haagen–Poiseuille one. When Pe is sufficiently small ($Pe \sim O(1)$), molecular diffusion acts in the transverse direction: the overall effect of both advection and transverse diffusion is a convection–diffusion process, in which the mixing zone is advected with the average flow velocity U_0, and spreads with an effective diffusion coefficient

$$D_{eff} = \frac{U_0^2 H^2}{210 D_m}, \tag{3.1}$$

https://doi.org/10.1017/S0022112097004928 Published online by Cambridge University Press

in the case of a flow between parallel plates (Turner 1959). The hydrodynamic dispersion process is described by a 'macroscopic' convection–diffusion equation, analogous to equation (2.11), in which $\boldsymbol{u}(\boldsymbol{r})$ is replaced by its mean $\boldsymbol{U}_0$, D_m by D_{eff} and the concentration field $C(\boldsymbol{r},t)$ by its transverse-averaged value $\bar{C}(x,t)$. At high *Pe*, diffusion has not enough time to mix the fluids, and the front region between the two fluids stretches linearly in time, due to the parabolic velocity field.

We show in figure 2 the results of simulations obtained after 20 000 time steps, over a wide range of *Pe* (from 0.5 to 512), in the case where the two fluids have the same viscosity ($M = 1$). The value of *Pe* is controlled by the value of D_m. The average concentration $\bar{C}(x,t)$ over a given cross-section accounts for the proportion of each fluid at that location. At small *Pe* (figure 2*a*, *Pe*= 0.5), we observe efficient mixing, resulting in an overall average concentration profile with a shape close to an error function, and a shape of the iso-concentration contours barely sensitive to the parabolic velocity profile. The average concentration profile can be analysed, using the solution of the convection–diffusion equation, with D_{eff} to be determined from a fit to the data. This has been achieved in figure 3, which shows the result of a simulation performed on the narrower lattice ($H = 16$), for $Pe = 0.8$. The figure displays a set of the average concentration, the iso-concentration contours, the velocity profiles along the sample, together with the theoretical and simulated transversely averaged concentrations. The agreement with the theory is very good, giving confidence in our lattice BGK approach. Note that the simulation on a lattice with 16 nodes in one direction gives satisfactory results concerning the concentration, as well as the velocity field.

Figure 2 also displays the evolution of the mixing process, as *Pe* increases. The iso-concentration contours become sharper and closer to one another. For a sufficiently high *Pe* (figure 2*e*,*f*, $Pe = 262$ and 512), we can consider that the fluids do not mix: indeed, not only is the shape of the iso-concentration contours reminiscent of the parabolic flow field, but the contours are very close to one another. We estimate the distance between the iso-concentration contours $C = 0.25$ and $C = 0.75$ in the case of the largest *Pe* ($Pe = 512$), to be of the order of three lattice units. In the following sections, we shall refer to the region separating the fluids as an interface (at high *Pe*). The region where the two fluids are present ($0 < \bar{C} < 1$ on the top plots) will be called the coexistence region.

It should be noticed that the high-*Pe* regime pertains to the case where molecular diffusion has not had enough time to homogenize the concentration in the transverse direction. In other words, this regime could be viewed as a 'transient' one, only insofar as one would need to wait a rather long time to see the effect of molecular diffusion. More precisely, if the simulation of figure 2(*f*) ($Pe = 512$) were extended over the same time interval (i.e. up to $t = 40\,000$), the pattern obtained would be the one corresponding to $Pe = 256$, that is roughly figure 2(*e*). This high-*Pe* regime is nonetheless of great interest, since it gives us the opportunity to study an interface in the absence of molecular diffusion.

3.2. *Case $M \neq 1$: the effect of the viscosity ratio*

When the viscosity ratio is different from 1, the velocity field is altered by the mixing process, inducing in turn changes in the concentration profiles. Here we shall compare the results obtained for $M = 100$ and $M = 0.01$ with the case $M = 1$. The Reynolds numbers for $M = 100$ and $M = 0.01$ are equal to 0.32 or 32, according to whether the viscosity used is that of the injected fluid or of the displaced one.

Let us focus on the case $M = 100$, corresponding to the displacement of a fluid of viscosity η_2 by a fluid of viscosity η_1 a hundred times smaller than η_2.

https://doi.org/10.1017/S0022112097004928 Published online by Cambridge University Press

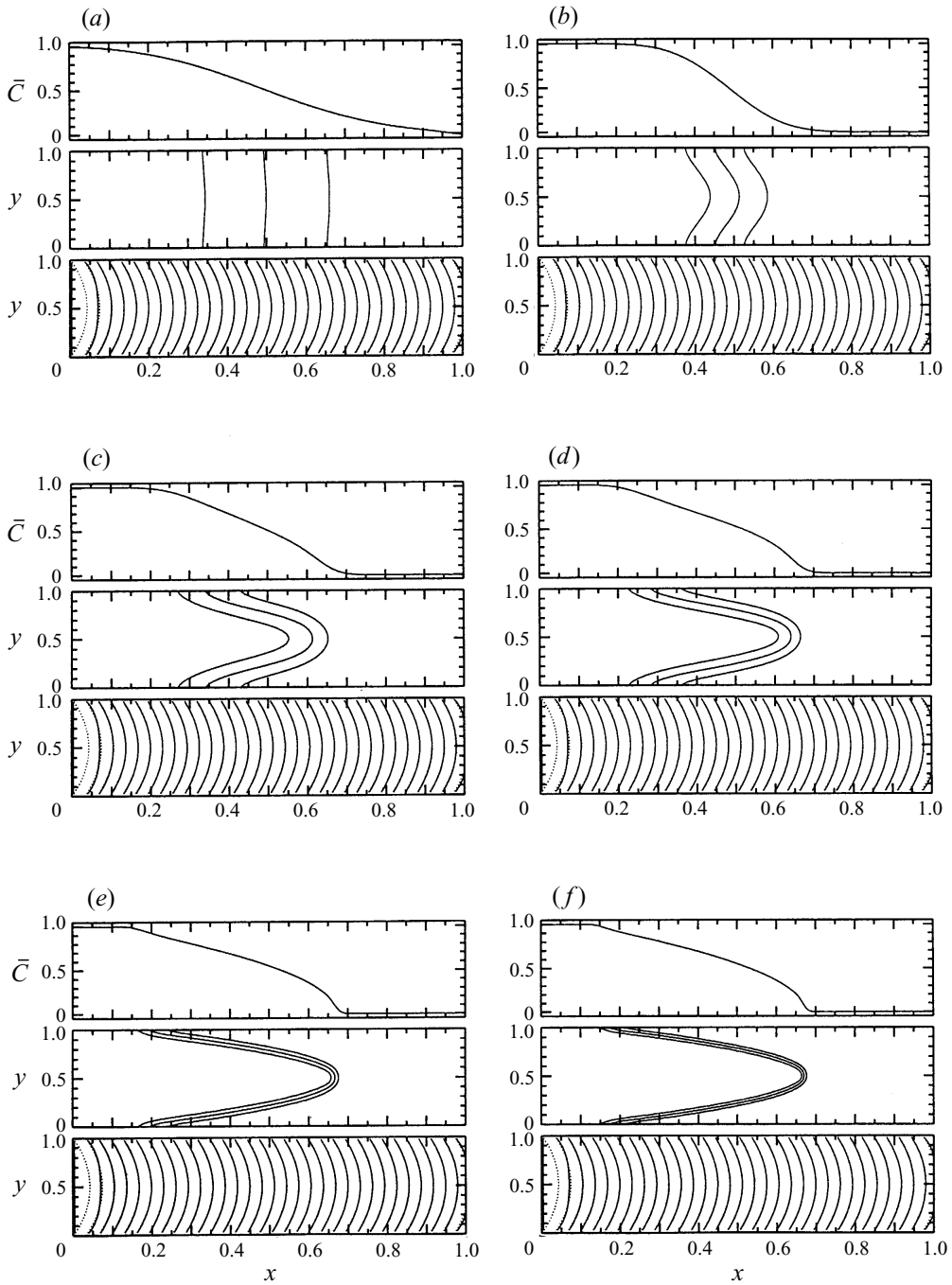


FIGURE 2. Mixing versus Péclet number for iso-viscosity fluids: $M = 1$. The value of Pe is controlled by the value of D_m. (From (*a*) to (*f*) $Pe = 0.5$; 5; 26; 51; 262; 512). On each data set, obtained at time $t = 20\,000$, the top plot shows the transverse-averaged concentration $\bar{C}$, the middle plot shows the iso-concentration contours $C = 0.25$, 0.5, 0.75, the bottom plot shows the longitudinal velocity profiles (solid lines) and the theoretical parabolic Haagen–Poiseuille profile, for the same flow rate (dots).

https://doi.org/10.1017/S0022112097004928 Published online by Cambridge University Press

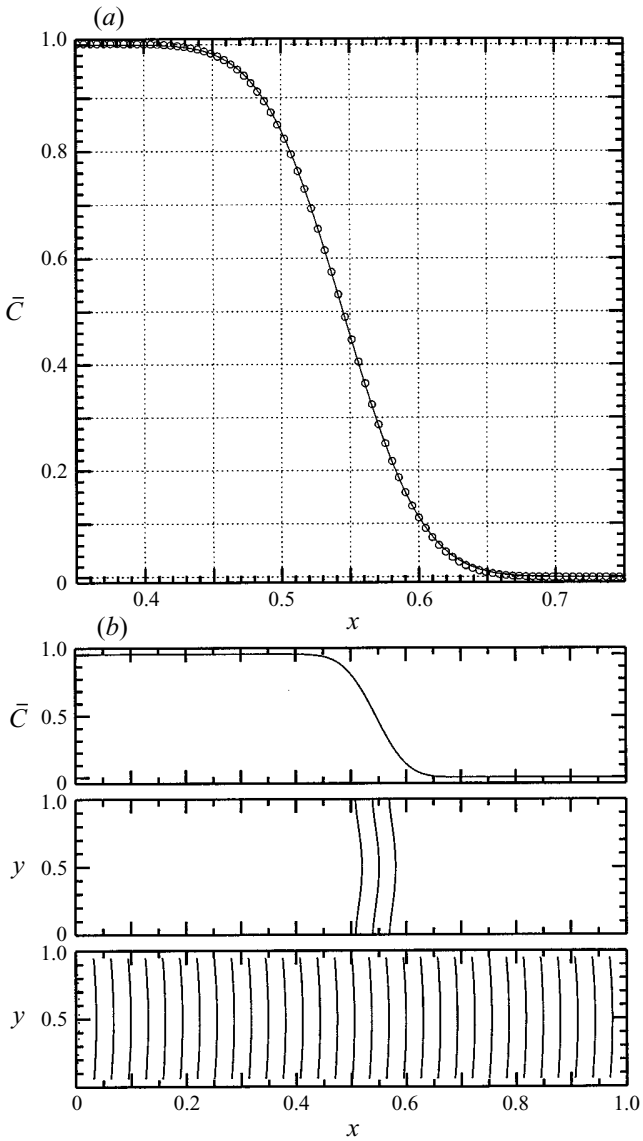


FIGURE 3. Taylor dispersion: $M = 1$; $Pe = 0.8$. Simulation performed on a lattice of size $H = 16$, $L = 2048$. (*a*) Transverse-averaged concentration versus the reduced distance in the flow direction. Open circles are from our numerical simulation; the solid line is the best theoretical complementary error function fit. The theoretical Taylor–Aris dispersion value D_{eff} is 0.14 and the fit gives $D_{eff} = 0.13$. (*b*) Same plots as in figure 2.

The results are displayed in figure 4, in a form similar to figure 2 (in particular, the *Pe* are the same). First we can notice that for *Pe* smaller than 1 (figure 4*a*), molecular diffusion is most dominant, resulting in the same average concentration, iso-concentration contours, and velocity profiles in the mixing region as in the case $M = 1$. When *Pe* is slightly increased (figure 4*b*, $Pe = 5$), a small deviation from a parabolic velocity profile appears, in the region between the pure fluids. As *Pe* is increased further, the deviation from the parabolic profile becomes more pronounced, and the iso-concentration contours get closer to one another. The extent

https://doi.org/10.1017/S0022112097004928 Published online by Cambridge University Press

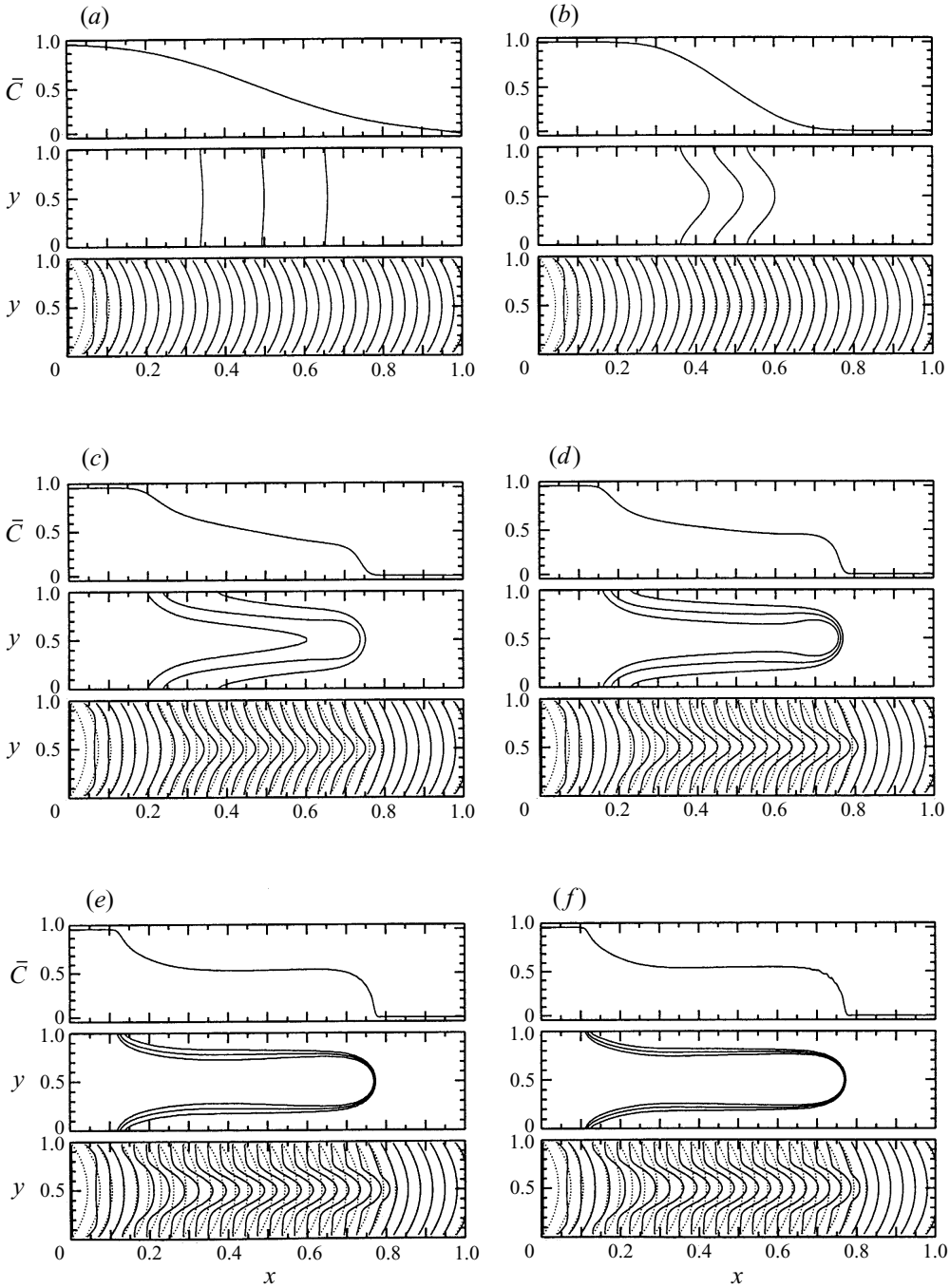


FIGURE 4. $M = 100$; $0.5 \leqslant Pe \leqslant 512$. Same plots as in figure 2.

of the region between the pure fluids is stretched in the flow direction, compared to the case $M = 1$. The last four data sets, figure 4(*c–f*), show the evolution toward a well-defined finger, obtained for $Pe \geqslant 262$ (figure 4*e*), and the stretching in the same way of the coexistence region, in the direction x. From now on we shall use the term finger when a plateau can be distinguished on the average concentration

https://doi.org/10.1017/S0022112097004928 Published online by Cambridge University Press

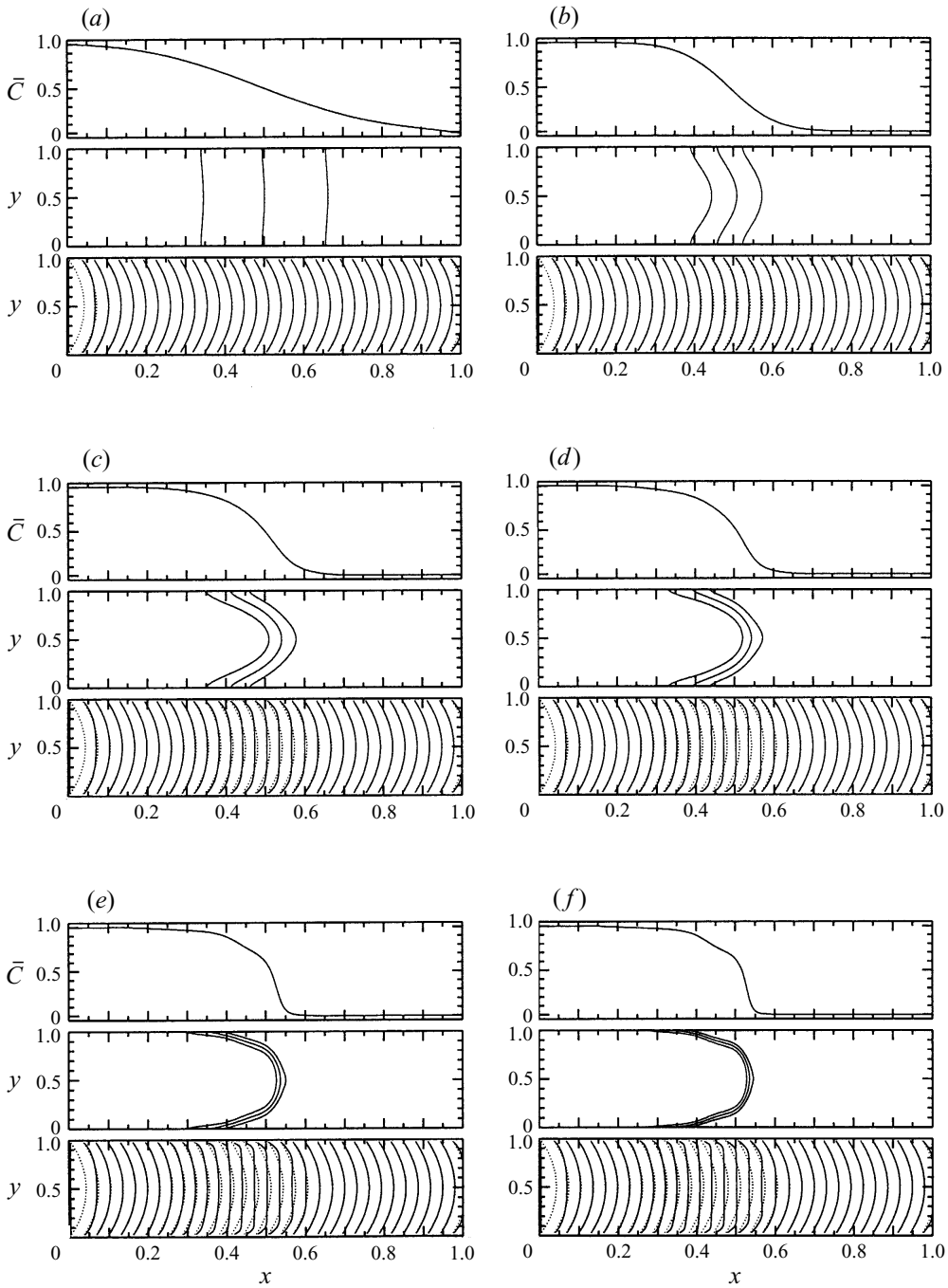


FIGURE 5. $M = 0.01$; $0.5 \leqslant Pe \leqslant 512$. Same plots as in figure 2.

plot. In addition, the average concentration profile is almost Pe-independent for values of Pe larger than 262, justifying the choice of the largest Pe in our simulations, while keeping Pe smaller than $Pe^* = 4v/D_m$ in order to avoid entrance effects.

The flow field is affected by the viscosity variations in the coexistence region: the

https://doi.org/10.1017/S0022112097004928 Published online by Cambridge University Press

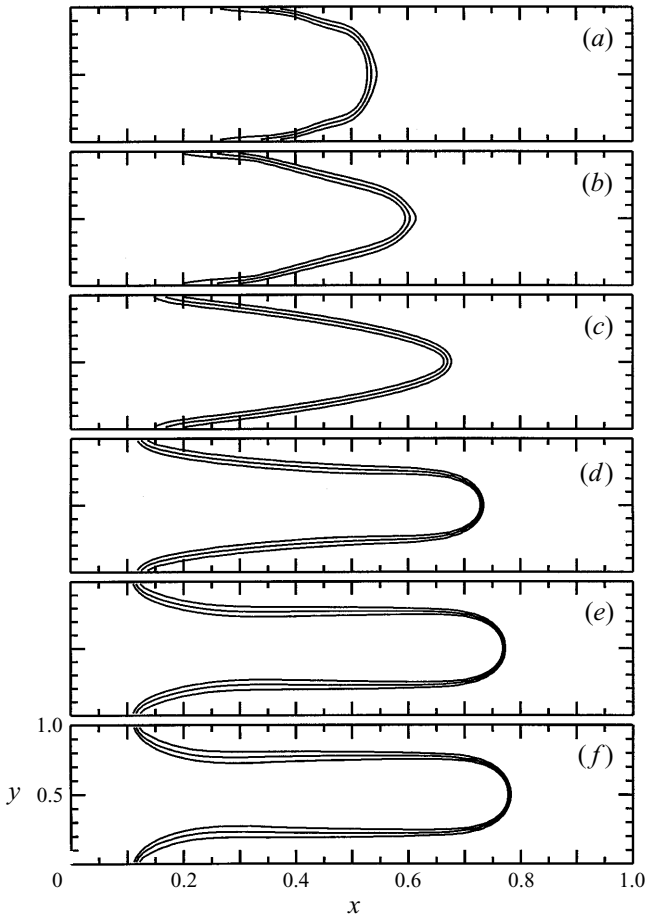


FIGURE 6. $Pe = 512$. (*a*)–(*g*) $M = 0.01; 0.1; 1; 10; 100; 1000$. Iso-concentration contours $C = 0.25$, 0.5, 0.75 obtained at time $t = 20\,000$.

x-component of the velocity is larger inside the less-viscous fluid (in the middle of the gap), and reduced inside the more-viscous fluid (in the vicinity of the walls), owing to the imposed constant flow rate. Both effects are enhanced as *Pe* is increased, resulting in a nearly flat velocity profile in the more-viscous fluid, far from the tip of the finger (figure 4*f*). Outside this region, Haagen–Poiseuille flow develops in the viscous fluid.

For a viscosity contrast smaller than 1 (see figure 5, $M = 0.01$), those tendencies are mainly reversed: compared to the case $M = 1$, the extent of the region between the pure fluids is smaller and the iso-concentration lines are almost equidistant. At large *Pe*, the velocity profile in the coexistence region is flatter inside the more viscous fluid (the flow approaches a plug flow). We note that for $M = 0.01$, entrance effects may possibly alter the concentration profile at high *Pe* (figure 5*e*, *f*, $Pe = 262$ and 512): indeed Pe^* is of the order of 200 (resp. 20 000) when evaluated with the viscosity of the displaced (resp. injected) fluid. The shoulder present above $\bar{C} \sim 0.6$ at $Pe = 512$ (figure 5*f*) will vanish at larger times, and the profile will turn into a smooth profile (figure 5*c*, *d*). A last remark concerning the case $M = 0.01$ is that it constitutes a limiting case insofar as it is difficult to obtain a very large *Pe* (corresponding to short times), while ensuring that no entrance effect is present.

https://doi.org/10.1017/S0022112097004928 Published online by Cambridge University Press

Figure 6 shows the iso-concentrations, $C = 0.25, 0.5, 0.75$, for values of M ranging over five decades in the high-Pe regime ($Pe = 512$). As mentioned above, for this value of Pe, the fluids have not had enough time to mix. Therefore, we shall analyse below the profile in terms of a well-defined interface between the two fluids, located on the iso-concentration contour $C = 0.5$.

3.3. *Time evolution of the interface at high Péclet numbers*

As mentioned in the introduction, large Pe provide a physical system where we can address the issue of pure viscous effects. We deal asymptotically with two miscible fluids without diffusion (infinite Pe), which is equivalent to immiscible fluids with no interfacial tension (infinite capillary number $Ca = U_0\,\eta/\gamma$, where γ is the interfacial tension). The shape of the frontier between the two fluids is the key issue of the problem, as it controls the dynamics of the macroscopic flow. Note that the interface can be determined either from the average concentration profile, or from the iso-concentration contour $C = 0.5$: in figures 2, 4 and 5 the top plot of each data set is equivalent to the upper half ($y \geqslant 0.5$) of the middle plot.

From the data sets of figure 7, obtained at $Pe = 512$, we can extract the main features to be analysed in more detail. Figure 7(*a*) shows the time evolution of the average concentration and of the iso-concentration contour $C = 0.5$, for $M = 100$. The front is mainly a finger travelling at a constant velocity U_{tip}, whereas the rear remains steady at the inlet. Therefore the mass conservation at constant flow rate gives a simple relation between the velocity of the finger tip and the finger width W:

$$\frac{U_0}{U_{tip}} = \frac{W}{H} = \lambda. \tag{3.2}$$

The average concentration from the plateau to the tip of the finger obeys the steady behaviour $\bar{C}(x,t) = \bar{C}(x - U_{tip}t)$.

At values of M of about 1, the feature is quite different: the interface seems to spread linearly in time (see figure 7*b*, $M = 1$). The average concentration is therefore expected to scale with a convective law $\bar{C}(x,t) = \bar{C}(x/t)$. However, it should be pointed out that large variations in the Péclet number (or equivalently very different times) may lead to a change in the flow regime; for this reason, we have plotted in figure 8 the interface obtained at time steps equal to $t = 14\,000$; $17\,000$ and $20\,000$ (for which Pe ranges between 731 and 512), versus the reduced variable x/t, for values of M equal to 0.2, 1, 5 and 10. The case $M = 1$ (figure 8*b*) shows that the curves are satisfactorily superimposed on one another, as expected. This is still the case if $Pe \gg 1$. Each average concentration $\bar{C}$ travels with its own velocity $u_{\bar{C}} = \left(\partial x/\partial t\right)_{\bar{C}}$, measured either on the time series of the average concentration $\bar{C}(x,t)$ (figure 7*b*), or on the time series of the iso-concentration contour $y(x,t)$, in the region $y \geqslant 0.5$ (figure 7*b*). When M is slightly increased (figure 8*c*, $M = 5$), a small deviation from the $\bar{C}(x/t)$ behaviour can be seen, in the region surrounding the front of the interface. Yet this deviation diminishes when time increases (time steps $t = 17\,000$ and $20\,000$ on the plot). The same feature is observed for values of M up to $M \sim 10$ (figure 8*d*). The above comments may be made for values of M slightly smaller than 1 (figure 8*a*, $M = 0.2$), down to $M \sim 0.1$; the difference with $M > 1$ lies in the fact that the deviation from the $\bar{C}(x/t)$ behaviour is visible mostly at the tip of the interface. When M is much smaller than 1 (see figure 7*c*, $M = 0.01$), the average concentration does not seem to scale as $\bar{C}(x,t) = \bar{C}(x/t)$; indeed the shape of the profile evolves in time. This may be due to the fact that the coexistence region is smaller than for the case $M \sim 1$, whereas the flow rate is

https://doi.org/10.1017/S0022112097004928 Published online by Cambridge University Press

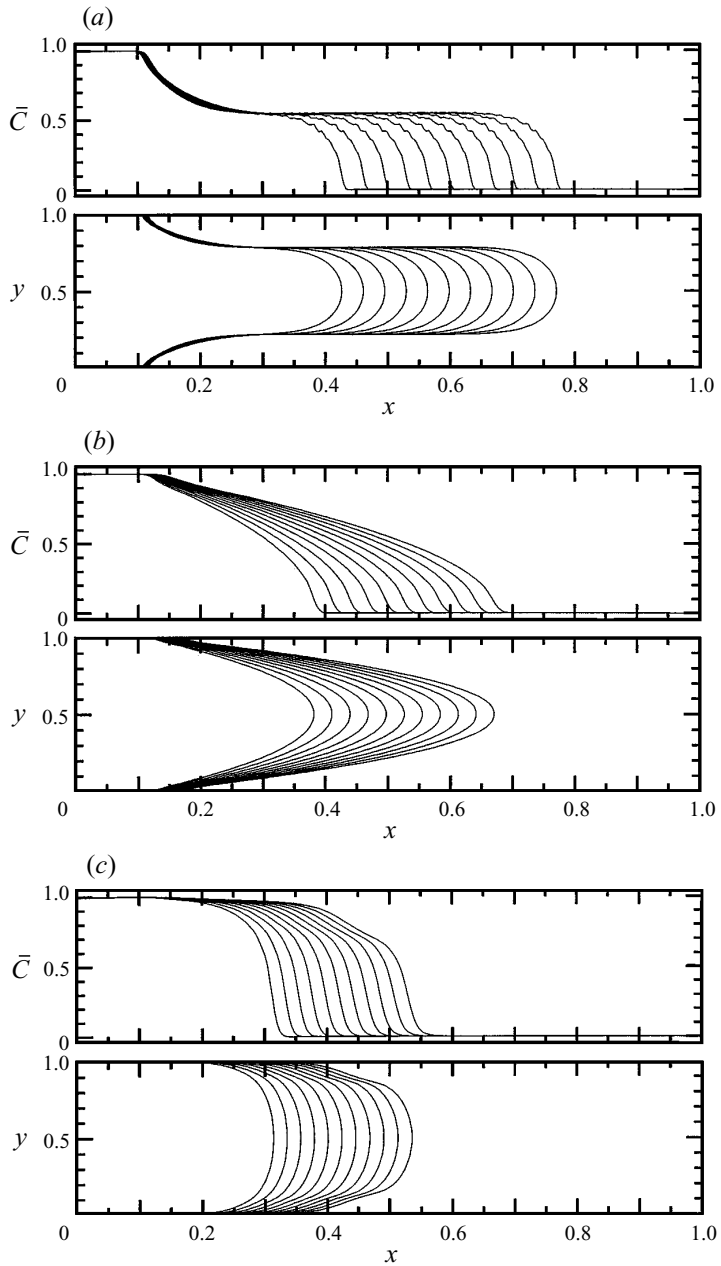


FIGURE 7. Transverse-averaged concentration and iso-concentration contour $C = 0.5$ at times t ranging between 10 000 and 20 000. (*a*) $M = 100$; $Pe = 512$. (*b*) $M = 1$; $Pe = 512$. (*c*) $M = 0.01$; $Pe = 512$.

the same: molecular diffusion will act on a narrower region and will therefore be more rapidly efficient. The only way to overcome this problem would be to increase the Péclet number, hence use a smaller molecular diffusion coefficient. Unfortunately the technique we use would reach its limitations (D_m must not be smaller than 10^{-4}).

The $\bar{C}(x/t)$ behaviour is reminiscent of the main recent results of Yang & Yort-

https://doi.org/10.1017/S0022112097004928 Published online by Cambridge University Press

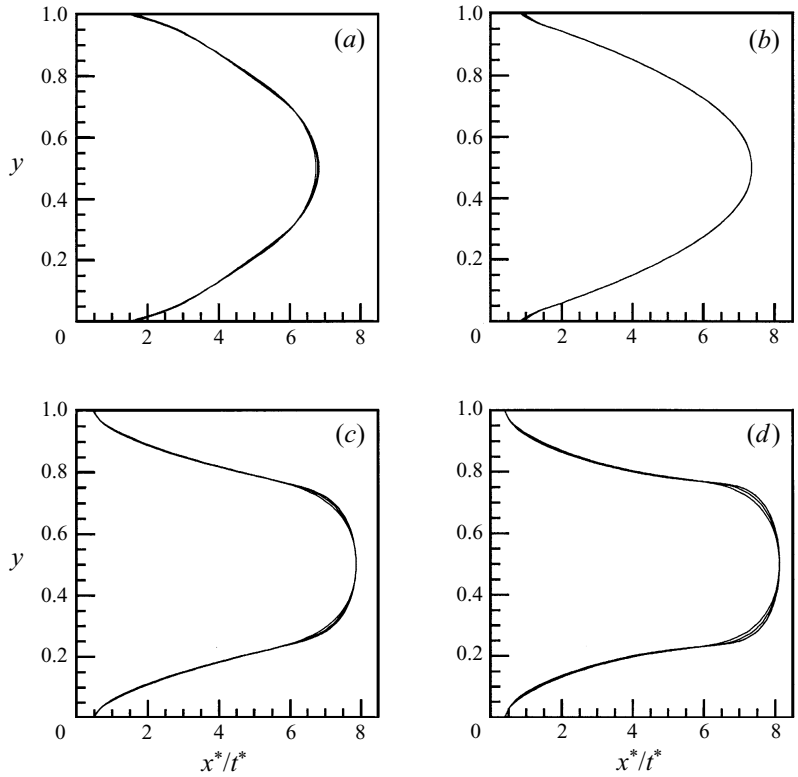


FIGURE 8. Plot of the iso-concentration contour $C = 0.5$ versus x^*/t^* (x^* is the distance travelled, $t^* = t/1{,}000$). Each data set displays the times $t = 14\,000$; $17\,000$; $20\,000$ superimposed. (*a*)–(*d*) $M = 0.2$; 1; 5; 10.

sos (1997), who performed the asymptotic analysis of the problem, in the limits of an infinite Péclet number and an infinite aspect ratio L/H, and under the condition of a Stokes flow. The flow reduces therefore to a parallel flow between two plates, and the average concentration $\bar{C}(x,t)$ is governed by the continuity equation:

$$\frac{\partial \bar{C}}{\partial t} + \frac{\mathrm{d}f_M(\bar{C})}{\mathrm{d}x} = 0, \tag{3.3}$$

where $f_M(\bar{C})$ is the flux of the injected fluid. The solution of this hyperbolic equation leads to the velocity of the average concentration $\bar{C}$:

$$\left(\frac{\partial x}{\partial t}\right)_{\bar{C}} = \frac{\mathrm{d}f_M(\bar{C})}{\mathrm{d}\bar{C}}. \tag{3.4}$$

The above equation predicts nothing less than the $\bar{C}(x/t)$ behaviour. Yang & Yortsos give an analytical solution to equation (3.4). In order to compare our data with their results, we plot in figure 9 $\bar{C}$ as a function of $\left(\partial x/\partial t\right)_{\bar{C}}/U_0$, for values of M ranging between 0.2 and 10, and also for $M = 100$. The plot is also a description of the evolution of the interface shape with M: as M increases, the interface stretches continuously until the finger appears. While figure 9 shows similar trends, our curves do not fit exactly on top of Yang & Yortsos's curves; the reason for this discrepancy may be that these authors work at infinite Péclet number and infinite aspect ratio

https://doi.org/10.1017/S0022112097004928 Published online by Cambridge University Press

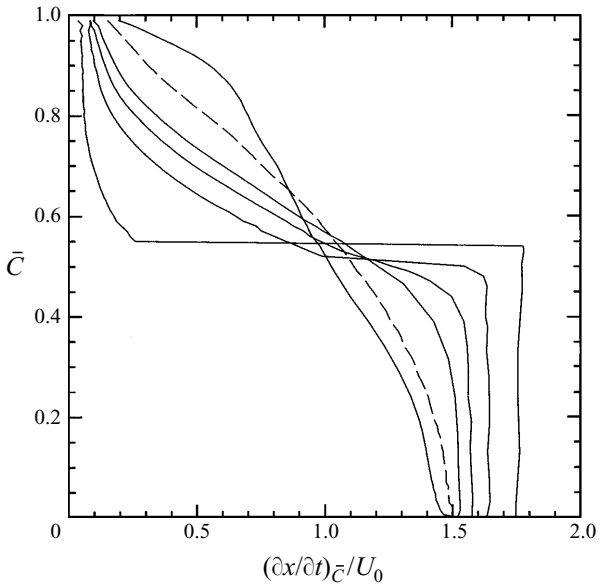


FIGURE 9. Transverse-averaged concentration $\bar{C}$ versus $(1/U_0)(\partial x/\partial t)_{\bar{C}}$ for $M = 0.2$; 1 (dashed); 3; 5; 10; 100 and $Pe = 512$.

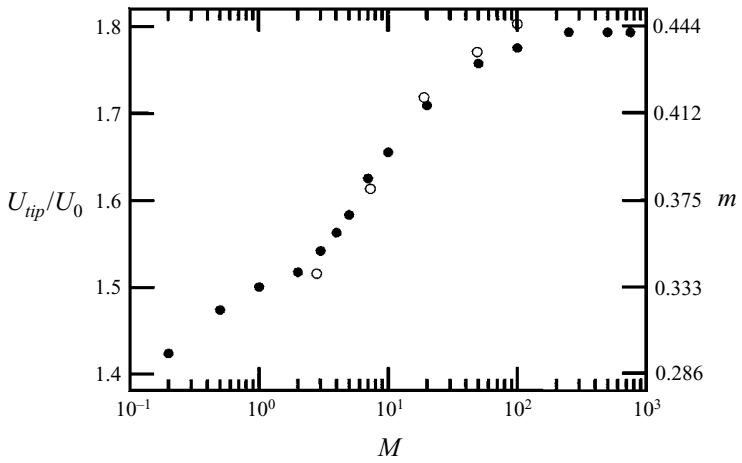


FIGURE 10. Reduced tip velocity U_{tip}/U_0 versus the viscosity ratio M (solid circles) for $Pe = 512$. The corresponding value of the fraction m of the film left behind is shown on the vertical axis on the right side of the figure. The open circles correspond to the data of Chen & Meiburg (1996).

L/H; unfortunately we have showed that we could not have in the same simulation both $Pe \gg 1$ and $L/H \longrightarrow \infty$.

3.4. *Characterization of the interface at large viscosity ratios and high Péclet numbers*

Figure 10 plots the reduced velocity of the finger tip U_{tip}/U_0 versus M. It increases slowly from 1.4 to 1.5 as M increases from low values to 1. U_{tip} increases slowly when M varies from 1 to 10. Above $M \sim 10$, it rises much faster and levels off at a value equal to 1.79 at large M. The latter value gives a reduced width of the finger, $\lambda = U_0/U_{tip} = 0.56$. The vertical axis on the right-hand side of the figure corresponds

https://doi.org/10.1017/S0022112097004928 Published online by Cambridge University Press

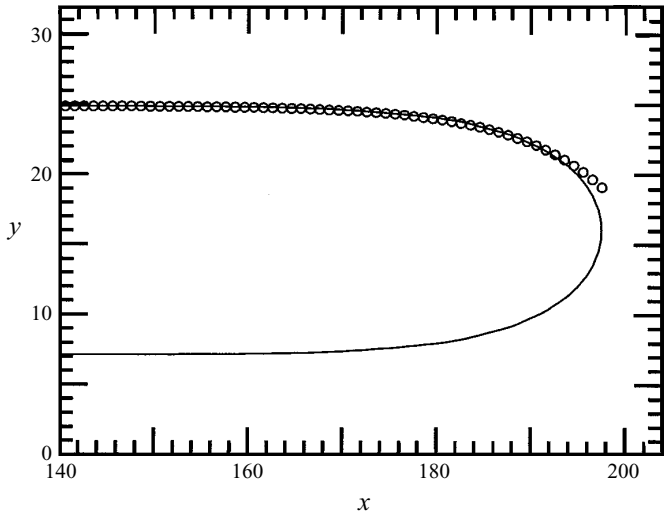


FIGURE 11. Fit of the rear of the finger obtained at $M = 100$ and $Pe = 512$, using the calculations of Reinelt & Saffman.

to the fraction m of the film left behind, given by

$$m = 1 - \lambda = 1 - \frac{U_0}{U_{tip}}. \tag{3.5}$$

The value of m can be compared with the results obtained by Chen & Meiburg (1996) with another numerical technique. We plot for this purpose in figure 10 (as open circles) their data; they are in reasonable agreement with ours, with an asymptotic value of m close to ours at large M.

We shall now focus on this limiting case. Tremendous efforts have been made to determine the shape of the finger, in the case of a potential flow (Saffman & Taylor 1958; Pitts 1980). We deal in this work with a viscous flow between parallel plates; our data have therefore to be compared with Reinelt & Saffman's (1985), who analysed the two-dimensional immiscible Stokes problem in the case $M \to \infty$, and for a finite capillary number Ca. Using a method of asymptotic matched expansions, they derived a shape for the finger given by $y \sim \lambda + A\exp(kx)$, in the region where its reduced width tends to a constant λ. In the above expression, the reference frame is moving with the finger, and the tip of the finger is fixed at the origin. This allowed them, using the interface and boundary conditions on the wall, to derive the relation between Ca, λ and k, the decay rate as $x \to -\infty$ (equation (20) in their work). We can probe their finger shape $y(x)$, using the constant A as a fitting parameter. In order to achieve the fitting procedure, we use our measured value of λ ($\lambda = 0.56$), and solve their relation between Ca, λ and k at high values of Ca (capillary forces negligible). This gives $\cos q = q$, where $q = k(1-\lambda)$, that is $q = 0.74$. The value of k to be used in the fit is then

$$k_{RS} = \frac{0.74}{1-\lambda} = 1.68. \tag{3.6}$$

Figure 11 shows the result of the fitting procedure. The shape of the rear of the finger obtained at $M = 100$ and $Pe = 512$ is correctly described by the curve $y = 0.56 + 0.36\exp(1.68\,x)$. Note that our value of λ is comparable with the one they would obtain at high values of Ca (figures 3 and 4 in their work). We have however

https://doi.org/10.1017/S0022112097004928 Published online by Cambridge University Press

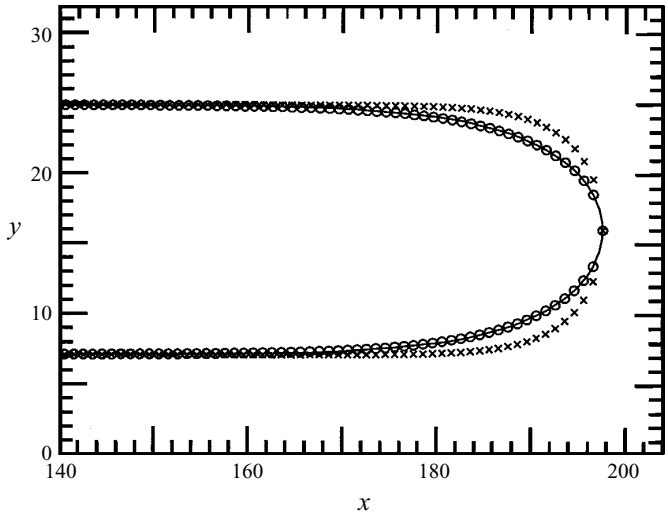


FIGURE 12. Fit of the viscous finger obtained at $M = 100$ and $Pe = 512$, using expression (3.9). The solid line is the result of our simulation, the crosses are the Saffman–Taylor formula obtained in a potential flow, the open circles are our fit with a measured reduced width $\lambda = 0.56$ and a decay rate $k_{RS} = 1.68$.

to go one step further, in order to derive the analytical expression for the entire finger. We shall for this purpose, recall Pitts's approach for fitting the shape of the Saffman–Taylor finger (Pitts 1980): in the class of closed form solutions developed from the original Saffman–Taylor approach, Pitts, in order to take capillary effects into account, tried a one-parameter α fit to his experimental data:

$$\exp\left(\frac{\pi x}{2\alpha}\right) = \cos\left(\frac{\pi y}{2\lambda}\right). \tag{3.7}$$

Such a solution, although extrapolated from the potential flow case, provides an analytical formula for the shape of the finger. In addition, the argument of the exponential term is the same as Reinelt & Saffman's one, provided that α is taken equal to $\pi/2k$. We hence attempt a fit to our data, using the expression of Pitts and the values $\lambda = 0.56$, $k_{RS} = 1.68$. This is achieved in figure 12 (circles). The result of the fitting procedure is excellent. Note that the asymptotic $y(x)$ of Reinelt & Saffman can be derived from Pitts's equation, through an expansion of the cosine term about $\pi/2$ (corresponding to $x \to -\infty$). The asymptote of Reinelt & Saffman then reads

$$y = \lambda + \frac{2\lambda}{\pi}\exp(kx). \tag{3.8}$$

The constant $2\lambda/\pi$, when evaluated with $\lambda = 0.56$, is equal to 0.356, a value very close to the fitting parameter A used in figure 11 ($A = 0.36$). We also note that the shape of the Saffman–Taylor finger in a potential flow is fitted by Pitts's expression, but with $\alpha_{ST} = 1 - \lambda$, that is $k_{ST} = \pi/2(1-\lambda) = 1.57/(1-\lambda)$. Comparing the prefactors in the expressions relating k to $1/(1-\lambda)$, 0.74 in our case, and 1.57 in the case of the Saffman–Taylor finger, we can deduce that the shape of the viscous finger in a viscous flow between two parallel plates is similar to that of the Saffman–Taylor finger in a potential flow (crosses in figure 12), but stretched with a numerical factor of 2.12 in the flow direction.

https://doi.org/10.1017/S0022112097004928 Published online by Cambridge University Press

To summarize, in the no-mixing limit ($Pe \to \infty$), we find an interface which is a steady-state-shaped finger of reduced width $\lambda_\infty = 0.56$, when $M \to \infty$. We can analytically account for its shape, using an extrapolation of Reinelt & Saffman's approach for immiscible fluids. Our analysis supports the contention that the two-dimensional viscous finger (miscible fluids with $Pe \to \infty$, or immiscible fluids with $Ca \to \infty$), is analytically fitted by

$$\exp(k_{RS}\, x) = \cos\left(\frac{\pi y}{2\lambda_\infty}\right). \tag{3.9}$$

We have addressed the issue of a flow between two parallel plates in a two-dimensional geometry: the full three-dimensional flow has yet to be studied and numerical simulations in a real Hele-Shaw cell are in progress.

4. Conclusion

Using a BGK lattice gas technique, on which we have superimposed a viscosity mixing rule, we have studied the two-dimensional displacement of miscible viscous fluids between two parallel plates. A wide range of viscosity ratios and Péclet numbers have been simultaneously covered. We show that in the case of viscous flows at high Pe, there exists a smooth threshold in the viscosity ratio M, below which the interface self-spreads and is displaced with the fluid velocity field, and above which a single tongue develops. The width of the tongue decreases as M increases, down to an asymptotic value. In this limit an analytical fit of the tip of the finger has been obtained, giving a formulation analogous to the Saffman–Taylor fingering pattern for non-potential flows.

We are indebted to Professors Y. C. Yortsos and M. Rabaud for stimulating discussions, and C.-Y. Chen and E. Meiburg for communication of their preprint. This work was partially supported by GDR CNRS *Systèmes hétérogènes complexes*. Computer time has been provided by the Centre National de Calcul Parallèle en Sciences de la Terre (CNCPST) and by the Institut du Développement et des Ressources en Informatique Scientifique (IDRIS).

REFERENCES

Appert, C. & d'Humières, D. 1995 Density profiles in a diphasic lattice-gas model. *Phys. Rev.* E **51**, 4335–4345.

Aris, R. 1956 Dispersion of a solute in a fluid flowing through a tube. *Proc. R. Soc. Lond.* A **235**, 67–77.

Bacri, J.-C., Rakotomalala, N., Salin, D. & Woumeni, R. 1992 Miscible viscous fingering: experiments versus continuum approach. *Phys. Fluids* A **4**, 1611–1619.

Bacri, J.-C., Salin, D. & Woumeni, R. 1991 Three-dimensional miscible viscous fingering in porous media. *Phys. Rev. Lett.* **67**, 2005–2008.

Baudet, C., Hulin, J.-P., Lallemand, P. & d'Humières, D. 1989 Lattice gas model: a model for the simulation of dispersion phenomena. *Phys. Fluids* **1**, 507–511.

Behrend, O., Harris, R. & Warren, P. B. 1994 Hydrodynamic behavior of lattice Boltzmann and lattice BGK models. *Phys. Rev.* E **50**, 4586–4595.

Bensimon, D., Kadanoff, L. P., Liang, S., Shraiman, B. I. & Tang, C. 1986 Viscous flow in two dimension. *Rev. Mod. Phys.* **58**, 977–999.

Benzi, R., Succi, S. & Vergassola, M. 1992 The lattice Boltzmann equation: theory and applications. *Phys. Rep.* **222**, 145–197.

https://doi.org/10.1017/S0022112097004928 Published online by Cambridge University Press

Bhatnagar, P. L., Gross, E. P. & Krook, M. 1954 A model for collision processes in gases. I. Small amplitude processes in charged and neutral one-component systems. *Phys. Rev.* **94**, 511–525.

Chen, C.-Y. & Meiburg, E. 1996 Miscible displacement in capillary tubes. Part 2. Numerical simulations. *J. Fluid Mech.* **326**, 57–90.

Chen, Y., Ohashi, H. & Akiyama, M. 1994 Thermal LBGK model without nonlinear deviations in macrohydrodynamic equations. *Phys. Rev.* E **50**, 2776–2783.

Flekkøy, E. G. 1993 Lattice BGK model for miscible fluids. *Phys. Rev.* E **47**, 4247–4271.

Flekkøy, E. G., Oxaal, U., Feder, J. & Jøssang, T. 1995 Hydrodynamic dispersion at stagnation points: simulations and experiments. *Phys. Rev.* E **52**, 4952–4962.

Frisch, U., Hasslacher, B. & Pomeau, Y. 1986 Lattice-gas automata for the Navier–Stokes equation. *Phys. Rev. Lett.* **56**, 1505–1508.

Hickernell, F. J. & Yortsos, Y. C. 1986 Linear stability of miscible displacement processes in porous media in the absence of dispersion. *Stud. Appl. Maths* **74**, 93–115.

Higuera, F. J. & Jimenez, J. 1989 Boltzmann approach to lattice gas simulations. *Europhys. Lett.* **9**, 663–668.

Homsy, G. M. 1987 Viscous fingering in porous media. *Ann. Rev. Fluid Mech.* **19**, 271–311.

Inamuro, T., Yoshino, M. & Ogino, F. 1995 A non-slip boundary condition for lattice Boltzmann simulations. *Phys. Fluids* **7**, 2928–2930.

Ladd, A. J. C. 1994*a* Numerical simulations of particulate suspensions via a discretized Boltzmann equation. Part 1. Theoretical foundation. *J. Fluid Mech.* **271**, 285–309.

Ladd, A. J. C. 1994*b* Numerical simulations of particulate suspensions via a discretized Boltzmann equation. Part 2. Numerical results. *J. Fluid Mech.* **271**, 311–339.

Landau, L. & Lifschitz, E. 1958 *Statistical Physics.* Pergamon Press.

Loggia, D., Rakotomalala, N., Salin, D. & Yortsos, Y. C. 1995 Evidence of new instability thresholds in miscible fluid flows. *Europhys. Lett.* **8**, 633–638.

Manickam, O. & Homsy, G. M. 1995 Fingering instabilities in vertical miscible displacement flows in porous media. *J. Fluid Mech.* **288**, 75–102.

McNamara, G. R. & Zanetti, G. 1988 Use of Boltzmann equation to simulate lattice gas automata. *Phys. Rev. Lett.* **61**, 2332–2335.

Paterson, L. 1985 Fingering with miscible fluids in a Hele Shaw cell. *Phys. Fluids* **28**, 26–30.

Pelcé, P. 1988 *Dynamic of Curved Fronts.* Academic Press.

Petitjeans, P. & Maxworthy, T. 1996 Miscible displacement in capillary tubes. Part 1. Experiments. *J. Fluid Mech.* **326**, 37–56.

Pitts, E. 1980 Penetration of fluid into a Hele–Saw cell: the Saffman–Taylor experiment. *J. Fluid Mech.* **97**, 53–64.

Qian, Y. H. 1990 Gaz sur réseau et théorie cinétique sur réseaux appliquée à l'équation de Navier–Stokes. PhD thesis, Université Paris 6.

Qian, Y. H., d'Humières, D. & Lallemand, P. 1992 Lattice BGK models for Navier–Stokes equation. *Europhys. Lett.* **17**, 479–484.

Rakotomalala, N., Salin, D. & Watzky, P. 1996*a* Simulations of viscous flows of complex fluids with a BGK lattice gas. *Phys. Fluids* **8**, 3200–3202.

Rakotomalala, N., Salin, D. & Watzky, P. 1996*b* "Saffman–Taylor" finger in two dimensional parallel viscous flow. Submitted to *Europhys. Lett.*

Reif, F. 1965 *Fundamental of Statistical and Thermal Physics.* McGraw Hill.

Reinelt, D. A. & Saffman, P. G. 1985 The penetration of a finger into a viscous fluid in a channel and tube. *SIAM J. Sci. Statist. Comput.* **6**, 542–561.

Rothman, D. H. & Zaleski, S. 1994 Lattice-gas models of phase separation: interfaces, phases transitions, and multiphase flow. *Rev. Mod. Phys.* **66**, 1417–1479.

Saffman, P. G. & Taylor, G. I. 1958 The penetration of a fluid into a porous medium or Hele-Shaw cell containing a more viscous liquid. *Proc. R. Soc. Lond.* A **245**, 312–329.

Taylor, G. I. 1953 Dispersion of soluble matter in solvent flowing slowly through a tube. *Proc. R. Soc. Lond.* A **219**, 186–203.

Turner, G. A. 1959 Frequency response of some illustrative models of porous media. *Chem. Engng Sci.* **10**, 14–21.

Wooding, R. A. 1969 Growth of fingers at an unstable diffusing interface in a porous medium or Hele–Saw cell. *J. Fluid Mech.* **39**, 477–495.

https://doi.org/10.1017/S0022112097004928 Published online by Cambridge University Press

YANG, Z. & YORTSOS, Y. C. 1997 Asymptotic solutions to miscible displacements in geometries of large aspect ratio. *Phys. Fluids* **9**, 286–298.

YORTSOS, Y. C. 1995 A theoretical analysis of vertical flow equilibrium. *Trans. Porous Media* **18**, 107–129.

YORTSOS, Y. C. & HICKERNELL, F. J. 1989 Linear stability of immiscible displacement in porous media. *SIAM J. Appl. Math.* **49**, 730–748.

https://doi.org/10.1017/S0022112097004928 Published online by Cambridge University Press